# *Predictable Mobility: A Statistical Approach for Planetary Surface Exploration Rovers in Uncertain Terrain*

# Predictable Mobility

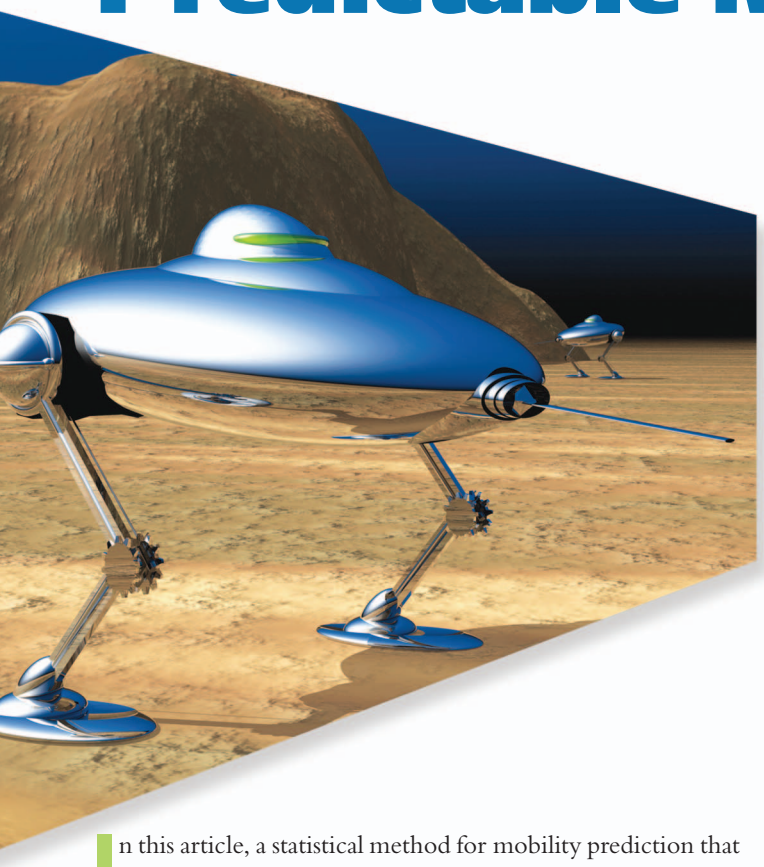

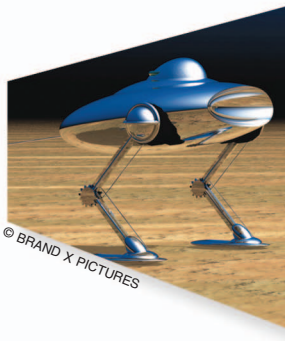


## *A Statistical Approach for Planetary Surface Exploration Rovers in Uncertain Terrain*

**BY GENYA ISHIGAMI, GAURAV KEWLANI, AND KARL IAGNEMMA**

In this article, a statistical method for mobility prediction that incorporates terrain uncertainty is presented. Mobile robotics has been performing a significant role in scientific lunar/planetary surface exploration missions [1]. In such missions, mobile robots are required to predict their mobility to avoid hazards such as immobilizing wheel slip on loose sand or collision with obstacles. This mobility prediction problem is thus important to the successful exploration on challenging terrain. Of particular interest is mobility prediction on sloped terrain, since travel on slopes can cause extreme longitudinal and lateral slips.

There have been significant works dealing with mobility predictions and analyses in the military community [2], [3]. These works have primarily focused on empirical analysis of large (i.e., several ton gross vehicle weight) vehicles. Other works have been performed to predict the mobility of small mobile robots while considering interaction mechanics of a slipping wheel on deformable terrain. Jain et al. have developed the rover analysis, modeling, and simulation software (ROAMS) simulator, which can be used for deterministic mobility prediction and includes models of terrain/vehicle interactions [4]. A multibody system for deterministic simulation of rover tire–soil interaction has also been demonstrated [5]. A terramechanics-based dynamic model for exploration rovers that considers slip and traction forces of a rigid wheel on deformable terrain has been developed [6].

These works have employed well-known dynamic and terramechanics models to calculate vehicle motion and wheel forces. However, these models assume prior knowledge of wheel–terrain interaction physical parameters (i.e., soil cohesion, internal friction angle, and others). In practical situations, mobile robots often traverse environments composed of terrain with unknown properties. These parameters can be estimated by onboard robotic sensor systems [7]–[9]; however, these estimated parameters remain subjected to uncertainty. Some recent work has attempted to predict rover mobility on slopes via a learning-based approach [10]; however, this work does not explicitly consider uncertainty in terrain physical parameters.

Based on these observations, it can be asserted that practical approaches to mobility prediction should explicitly consider uncertainty in terrain physical parameters. A conventional technique for estimating probability density function of a system's output response from uncertain input distributions is the Monte Carlo method [11], [12]. This approach generally requires a large number of analytical or numerical simulation trials to obtain a probability distribution of an output metric(s) associated with ranges of uncertain input parameters. Monte Carlo methods are typically computationally expensive, with computational cost increasing as the simulation model complexity increases. Structured sampling techniques such as Latin hypercube sampling, importance sampling, and others can be used to improve computational efficiency; however, these gains may be modest for complex problems [13], [14].

Alternatively, extended Kalman filters (EKFs) or particle filers have been well used for the prediction of a robot's position

*Digital Object Identifier 10.1109/MRA.2009.934823*


1070-9932/09/$26.00©2009 IEEE

***Mobile robotics has been performing a significant role in scientific lunar/planetary surface exploration missions.***

in uncertain environments, as mentioned in [15] and [16]; however, EKFs cannot explicitly deal with uncertainty on individual parameters. The particle filter is known as sequential Monte Carlo method, which needs a sensor model [i.e., global positioning system (GPS) or light detection and ranging (LIDAR) observations] to successively resample particles in high probability regions. Such an approach is not suitable for prior prediction of mobility before a rover travels in uncertain terrain.

This article proposes a statistical method for efficient mobility prediction consisting of two techniques: 1) a wheeled vehicle model for calculating wheel–terrain interaction forces and vehicle dynamic motions [6] and 2) a stochastic response surface method (SRSM) for modeling of uncertainty [17]–[19]. In the wheeled vehicle model, a terramechanics-based approach is used to calculate interaction forces of slipping wheels on deformable soil, and a dynamic model is employed to simulate vehicle motion. An SRSM is used as a functional approximation technique to obtain an equivalent system model with reduced complexity. Generally, the use of SRSM can reduce the number and complexity of model simulation trials to generate output metric statistics, when compared with Monte Carlo methods. In this article, the computational efficiency of SRSM is confirmed through the comparison with those of standard Monte Carlo (SMC) method and Latin hypercube sampling Monte Carlo (LHSMC) method.

Experimental studies of the proposed statistical mobility prediction method are conducted for a slope-traversal scenario in two different terrains. Here, two key terrain parameters, cohesion and internal friction angle, are chosen as uncertain parameters. The proposed method provides a prediction of rover motion, with confidence ellipses indicating probability ranges of the predicted position due to terrain parameter uncertainty. Further, the method predicts the rover's probable orientation and wheel slippage.

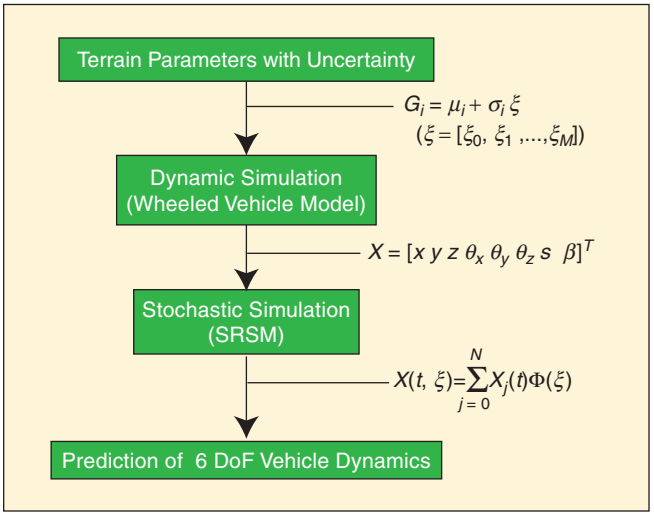


***Figure 1.*** *Flowchart of statistical mobility prediction method.*

## Outline of Statistical Mobility Prediction Method

Figure 1 shows a flowchart of the statistical mobility prediction method proposed in this article. This method is divided into three steps: First, uncertainty in terrain parameters $\boldsymbol{G}_i$ is represented as functions of standard random valuables (i.e., Gaussian variables):

$$\boldsymbol{G}_i = \mu_i + \sigma_i \boldsymbol{\xi}, \tag{1}$$

where $\mu_i$ is the mean, $\sigma_i$ is the standard deviation, and $\boldsymbol{\xi}$ is a set of standard normal random variables. Following the approach of [18], $M$ sample points are calculated, where $M$ is approximately twice the number of coefficients in SRSM reduced model (2).

In the second step, $M$ dynamic simulations using the wheeled vehicle model are carried out to obtain several values for the variables of interest in a state space $\boldsymbol{X}$ corresponding to the uncertain inputs $\boldsymbol{G}_i$. The state space $\mathbf{X}$ consists of state variables of the vehicle, for example, vehicle position and orientation, or wheel slippage.

In the third step, SRSM is employed to develop an equivalent reduced model of the state space, which can be expressed by

$$\boldsymbol{X}(t, \boldsymbol{\xi}) = \sum_{j=0}^{N} \boldsymbol{X}_j(t)\Phi_j(\boldsymbol{\xi}), \tag{2}$$

where $\boldsymbol{X}_j(t)$ is a set of unknown coefficient values that are calculated via a regression-based approach [18]. The number of unknown coefficients $(N + 1)$ is determined by both the degree $q$ of polynomial expansion (4) and the number of uncertain parameters. Once the coefficients are determined, the vehicle dynamic motion with terrain uncertainties can be predicted using the reduced model.

## Uncertainty Analysis Approach

### *Monte Carlo Method and Latin Hypercube Sampling*

Monte Carlo methods are well-known techniques for estimating a probability distribution of a system's output response from uncertain input parameters [11], [12]. A typical calculation step of Monte Carlo method to obtain the model output statistics is as follows: first, uncertain input parameters for an analytical or numerical system model are randomly sampled from their respective probability distributions. Then, multiple simulation runs are conducted using each set of the input parameter values to obtain the corresponding outputs for each case. The probability distribution of a user-defined output metric can then be generated while estimating various statistics such as mean and variance.

In the SMC method, since random sampling of the input parameter distributions is required, the number of simulation runs must be large enough to ensure representation of the

entire input parameter range and also to converge to the output distribution.

Several methods for efficient sampling of input parameters from their probability distributions have been developed. The LHSMC method [13], [14] ensures dense coverage of each input parameter's range by dividing the range into disjoint intervals of equal probability and then randomly sampling a parameter value from each interval (Figure 2). This approach reduces the number of samples of input parameters due to this efficient sampling technique and is thus an improvement over the SMC method in terms of computational cost.

### Stochastic Response Surface Method

SRSM provides a computationally efficient method for uncertainty propagation through the determination of a statistically equivalent reduced model [17], [18]. In SRSM, inputs to a system model may be given as functions of independent identically distributed (iid) normal random variables, each having zero mean and unit variance [e.g., as defined in (1)]. The same set of input random variables is then used for deriving the statistics of system model outputs.

An equivalent reduced model for output metrics is expressed as a series expansion in terms of standard random valuables as multidimensional Hermite polynomials with normal random variables

$$y = a_0 + \sum_{i_1=1}^{n} a_{i_1}\Gamma_1(\xi_{i_1}) + \sum_{i_1=1}^{n}\sum_{i_2=1}^{i_1} a_{i_1}a_{i_2}\Gamma_2(\xi_{i_1},\xi_{i_2}) + \cdots, \tag{3}$$

where $y$ is an output metric, $a_{i1}, a_{i2}, \ldots$ are unknown coefficients to be determined, and $\xi_{i1}, \xi_{i2}, \ldots$ are iid normal random variables. The Hermite polynomial of degree $q$ is given as

$$\Gamma_q(\xi_{i_1},\xi_{i_2},\ldots,\xi_{i_q}) = (-1)^q e^{\frac{1}{2}\boldsymbol{\xi}^T\boldsymbol{\xi}} \times \frac{\partial^q}{\partial\xi_{i_1},\ldots,\partial\xi_{i_q}} \times e^{-\frac{1}{2}\boldsymbol{\xi}^T\boldsymbol{\xi}}. \tag{4}$$

For notational simplicity, the series in (3) may be rewritten as shown in (2) as

$$y(t,\boldsymbol{\xi}) = \sum_{j=0}^{N} y_j(t)\Phi_j(\boldsymbol{\xi}), \tag{5}$$

where the series is truncated to a finite number of terms, and there exists a correspondence between $\Gamma_q(\xi_{i1}, \xi_{i2}, \ldots, \xi_{iq})$ and $\Phi_j(\xi)$ and their corresponding coefficients. In this article, the Hermite polynomial is used as an equivalent reduced model since input random variables are assumed to be Gaussian variables; however, different orthogonal polynomial basis functions can also be used for the probability distribution of other non-Gaussian variables [19].

The series expansion contains unknown coefficient values that can be determined from a limited number of system model simulations to generate an approximate reduced model. A set of sample points is selected, and model outputs at these points are used for calculating the unknown coefficients [18]. Once the statistically equivalent reduced model is formulated, it can be used to determine statistical properties related to mobility prediction, such as position and orientation of the vehicle subject to uncertainty. Note that the accuracy of the model output increases as the order of the expansion increases.

### Application of SRSM to Rover Mobility Prediction

In this article, two key terrain parameters, cohesion $c$ and internal friction angle $\phi$, are chosen as uncertain variables. These parameters were chosen because of their influence on maximum terrain shear strength. These uncertain parameters are defined by the following normal distributions:

$$\left.\begin{aligned} c &= \mu_c + \sigma_c\xi_c \\ \phi &= \mu_\phi + \sigma_\phi\xi_\phi \end{aligned}\right\}, \tag{6}$$

where $\mu_c$ and $\mu_\phi$ are the means, $\sigma_c$ and $\sigma_\phi$ are standard deviations, and $\xi_c$ and $\xi_\phi$ are standard normal random valuables.

The output metrics considered in this article include vehicle position, orientation, and wheel slippage, expressed as second-order multidimensional Hermite polynomials:

$$\begin{aligned}\boldsymbol{X}(t,\xi) = {} & \boldsymbol{X}_0(t) + \boldsymbol{X}_1(t)\xi_c + \boldsymbol{X}_2(t)\xi_\phi \\ & + \boldsymbol{X}_3(t)(\xi_c^2 - 1) + \boldsymbol{X}_4(t)(\xi_\phi^2 - 1) + \boldsymbol{X}_5(t)\xi_c\xi_\phi, \end{aligned} \tag{7}$$

where $\boldsymbol{X}_0(t), \ldots, \boldsymbol{X}_5(t)$ are the unknown coefficient matrices.

The state-space $\boldsymbol{X}$ is then defined as

$$\boldsymbol{X} = [\,x \quad y \quad z \quad \theta_x \quad \theta_x \quad \theta_x \quad \mathbf{s} \quad \boldsymbol{\beta}\,], \tag{8}$$

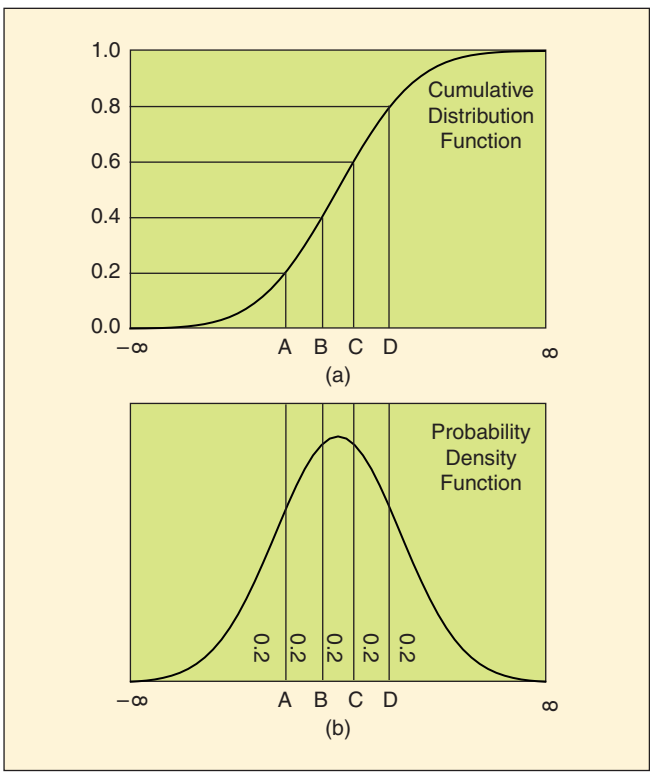


***Figure 2.*** *Illustration of sampling using the Latin hypercube sampling method.*

where $(x, y, z)$ are the vehicle position, $(\theta_x, \theta_y, \theta_z)$ are the vehicle orientation, and $\mathbf{s}$ and $\boldsymbol{\beta}$ include the slip ratios and slip angles of each individual wheel, which are respectively defined in (19) and (20) later.

Spectral stochastic analysis [20], [21] is then performed using the expansion defined in (7) to obtain time-series predictions of the motion path of the rover, vehicle orientations, and wheel slippages.

### Confidence Ellipse Calculation

Statistical techniques, such as Monte Carlo method and SRSM, can provide predicted rover path coordinates $(x, y)$ under uncertainty. Relevant output statistics such as mean, variances, and covariance can also be calculated. Based on these statistics, the motion path (here taken as the mean path) can be augmented with ellipses defined by the variances and covariance (see Figure 3). The ellipses indicate confidence levels for the predicted position on the path. The technique for confidence ellipse calculation is drawn from the method presented in [22].

Given a sufficient sample size $n$ from Monte Carlo method or SRSM of motion path coordinates $\mathbf{x}_i = [x_i,\ y_i]^T$, a sample mean vector $\bar{\mathbf{x}}$ is given as

$$\bar{\mathbf{x}} = [\bar{x},\ \bar{y}]^T, \tag{9}$$

where

$$\bar{x} = \frac{1}{n}\sum_{i=1}^{n} x_i, \quad \bar{y} = \frac{1}{n}\sum_{i=1}^{n} y_i. \tag{10}$$

The sample covariance matrix $\mathbf{S}$ is then determined as

$$\mathbf{S} = \frac{1}{n-1}\sum_{i=1}^{n} (\mathbf{x}_i - \bar{\mathbf{x}})(\mathbf{x}_i - \bar{\mathbf{x}})^T = \begin{bmatrix} s_x^2 & rs_x s_y \\ rs_x s_y & s_y^2 \end{bmatrix}, \tag{11}$$

where $s_x$ and $s_y$ are the sample standard deviations, $s_{xy}$ the sample covariance, and $r$ the sample correlation index. Then, the equation for a confidence ellipse is formulated by the following equation:

$$(\mathbf{x} - \bar{\mathbf{x}})^T \mathbf{S}^{-1} (\mathbf{x} - \bar{\mathbf{x}}) = C^2, \tag{12}$$

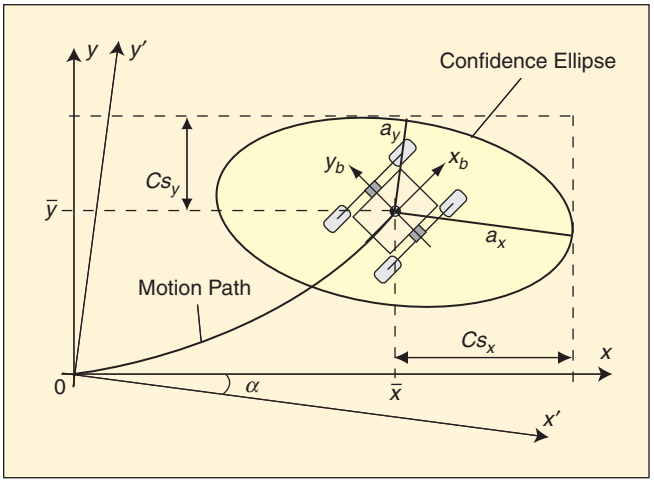


***Figure 3.*** *Confidence ellipse on the predicted motion path of the vehicle.*

where

$$C = \sqrt{-2\ \ln(1 - P)}, \tag{13}$$

and $P$ is the probability that determines the confidence level of the predicted position.

Then, (12) can be rewritten by substituting (9) and (11):

$$\frac{1}{1-r^2}\left[\frac{(x-\bar{x})^2}{s_x^2} - \frac{2r(x-\bar{x})(y-\bar{y})}{s_x s_y} + \frac{(y-\bar{y})^2}{s_y^2}\right] = C^2. \tag{14}$$

As illustrated in Figure 3, the principal semiaxes of the confidence ellipse for a given probability $P$ are obtained from the following relationships:

$$a_x = Cs'_x, \quad a_y = Cs'_y, \tag{15}$$

where $a_x$ and $a_y$ denote the major and minor semiaxes of the confidence ellipse. $s'_x$ and $s'_y$ are expressed by

$$\left.\begin{aligned} s'_x &= \left\{\left[s_x^2 + s_y^2 + \sqrt{(s_x^2 - s_y^2)^2 + 4r^2 s_x^2 s_y^2}\right]/2\right\}^{1/2} \\ s'_y &= \left\{\left[s_x^2 + s_y^2 - \sqrt{(s_x^2 - s_y^2)^2 + 4r^2 s_x^2 s_y^2}\right]/2\right\}^{1/2} \end{aligned}\right\}. \tag{16}$$

The orientation of the confidence ellipse with regard to the $x$-$y$ coordinate is defined by the inclination angle

$$\alpha = \frac{1}{2}\ \tan^{-1}\frac{2rs_x s_y}{s_x^2 - s_y^2}. \tag{17}$$

## Wheeled Vehicle Model

Dynamic simulation of a wheeled rover requires two submodels: a vehicle dynamic model of the rover to obtain several values for each state space variable and a wheel–terrain contact model to calculate the interaction forces of a wheel on deformable soil at each dynamic simulation step.

### Vehicle Dynamic Model

Here, a rover is modeled as an articulated multibody system. The vehicle addressed in this article is assumed to be a four-wheeled vehicle, as shown in Figure 4.

The dynamic motion of a vehicle for the given traveling and steering conditions are numerically obtained by successively solving the following motion equation:

$$\boldsymbol{H}\begin{bmatrix} \dot{\boldsymbol{v}}_0 \\ \dot{\boldsymbol{\omega}}_0 \\ \ddot{\boldsymbol{q}} \end{bmatrix} + \boldsymbol{C} + \boldsymbol{G} = \begin{bmatrix} \boldsymbol{F}_0 \\ \boldsymbol{N}_0 \\ \boldsymbol{\tau} \end{bmatrix} + \boldsymbol{J}^T \begin{bmatrix} \boldsymbol{F}_e \\ \boldsymbol{N}_e \end{bmatrix}, \tag{18}$$

where $\boldsymbol{H}$ represents the inertia matrix of each body, $\boldsymbol{C}$ is the velocity-depending term, $\boldsymbol{G}$ is the gravity term, $\boldsymbol{v}_0$ is the translational velocity of the vehicle, $\boldsymbol{\omega}_0$ is the angular velocity of the vehicle, $\boldsymbol{q}$ is the angle of each joint (such as wheel rotation and steering angle), $\boldsymbol{F}_0 = [0, 0, 0]^T$ is the forces at the centroid of the vehicle body, $\boldsymbol{N}_0 = [0, 0, 0]^T$ is the moment at the centroid

of the vehicle body, $\boldsymbol{\tau}$ is the torques acting at each joint (wheel/steering torques), $\boldsymbol{J}$ is the Jacobian matrix, and $\boldsymbol{F}_e$ is the external forces acting at the centroid of each wheel. The wheel–terrain contact model, as described in (21)–(23) later, calculates each external force. $\boldsymbol{N}_e$ is the external moment acting at the centroid of each wheel.

The vehicle dynamic model is required to be equivalent to the kinematic/dynamic parameters (i.e., geometric dimensions, mass, inertia, and others) of the corresponding vehicle addressed in the mobility prediction algorithm.

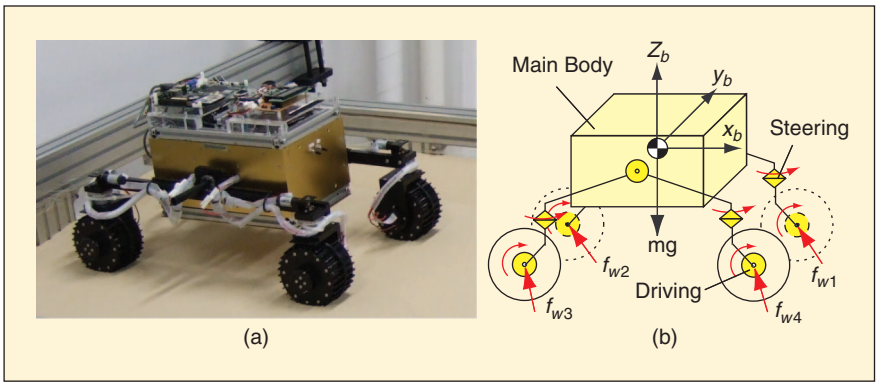


***Figure 4.*** *Vehicle dynamic model as an articulated multibody system. (a) Rover test bed. (b) Vehicle dynamic model.*

### *Wheel–Terrain Contact Model*

Wheel–terrain interaction mechanics has been well investigated in the field of terramechanics [23], [24]. A model for a rigid wheel traveling on deformable soil is shown in Figure 5. A wheel coordinate system is defined as a right-hand frame; in this system, the longitudinal direction is denoted by $x_w$, the lateral direction by $y_w$, and the vertical direction by $z_w$.

The slip ratio (i.e., slip in the longitudinal direction of wheel travel) is defined as a function of the longitudinal traveling velocity of the wheel $v_x$ and the circumferential velocity of the wheel $r\omega$, where $r$ is the wheel radius and $\omega$ represents the angular velocity of the wheel:

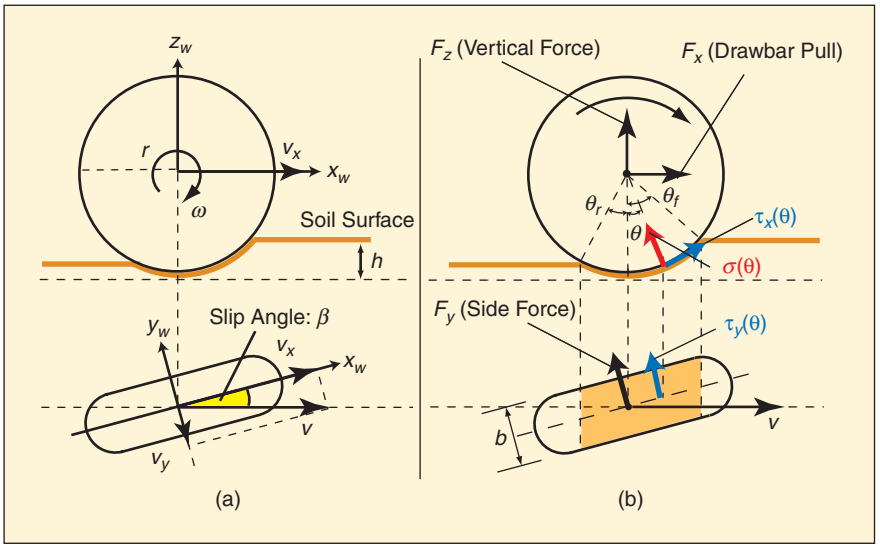


***Figure 5.*** *Wheel–terrain contact model to calculate drawbar pull, side force, and vertical force. (a) Wheel coordinate system and (b) wheel contact forces.*

$$\mathbf{s} = \begin{cases} (r\omega - v_x)/r\omega & (|r\omega| \geq |v_x|\text{: driving}) \\ (r\omega - v_x)/v_x & (|r\omega| < |v_x|\text{: braking}). \end{cases} \tag{19}$$

The slip ratio assumes a value in the range from $-1$ to 1.

The slip angle expresses the slip in the lateral direction of wheel, and it is defined as a function of $v_x$ and the lateral traveling velocity $v_y$ as follows:

$$\boldsymbol{\beta} = \tan^{-1}(v_y/v_x). \tag{20}$$

Wheel–terrain contact forces, including the drawbar pull $F_x$, side force $F_y$, and vertical force $F_z$, can be calculated by the following equations [6], [24]:

$$F_x = rb\int_{\theta_r}^{\theta_f} \{\tau_x(\theta)\cos\theta - \sigma(\theta)\sin\theta\}d\theta, \tag{21}$$

$$F_y = \int_{\theta_r}^{\theta_f} \{rb\tau_y(\theta) + R_b[r - h(\theta)\cos\theta]\}d\theta, \tag{22}$$

$$F_z = rb\int_{\theta_r}^{\theta_f} \{\tau_x(\theta)\sin\theta + \sigma(\theta)\cos\theta\}d\theta, \tag{23}$$

where $b$ represents the wheel width, $\sigma(\theta)$ the normal stress beneath the wheel, $\tau_x(\theta)$ and $\tau_y(\theta)$ are the shear stresses in the longitudinal and lateral direction of the wheel. The contact patch of the wheel is determined by the entry angle $\theta_f$ and exit angle $\theta_r$. $R_b$ is modeled as a reaction resistance generated by the bulldozing phenomenon on a side wall of the wheel [6]. $R_b$ is a function of wheel sinkage $h$. Also, $\sigma(\theta)$, $\tau_x(\theta)$, and $\tau_y(\theta)$ are defined by the following equations [24]:

$$\sigma(\theta) = \begin{cases} (ck_c + \rho bk_\phi)\left(\dfrac{r}{b}\right)^n(\cos\theta - \cos\theta_f)^n & (\theta_m \leq \theta < \theta_f) \\ (ck_c + \rho bk_\phi)\left(\dfrac{r}{b}\right)^n & \\ \quad \left\{\cos\left[\theta_f - \dfrac{(\theta - \theta_r)(\theta_f - \theta_m)}{\theta_m - \theta_r}\right] - \cos\theta_f\right\}^n, & \\ \quad (\theta_r < \theta \leq \theta_m) & \end{cases} \tag{24}$$

$$\left.\begin{aligned} \tau_x(\theta) &= [c + \sigma(\theta)\tan\phi][1 - e^{-j_x(\theta)/k_x}] \\ \tau_y(\theta) &= [c + \sigma(\theta)\tan\phi][1 - e^{-j_y(\theta)/k_y}] \end{aligned}\right\}, \tag{25}$$

where $k_c$ and $k_\phi$ represent the pressure sinkage moduli, $\rho$ is the soil density, $n$ is the sinkage exponent, $\theta_m$ is the maximum

***SRSM provides a computationally efficient method for uncertainty propagation through the determination of a statistically equivalent reduced model.***

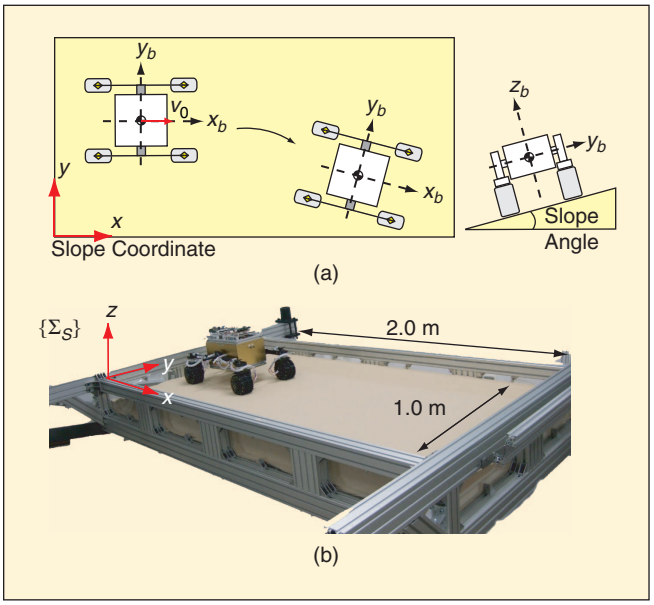


***Figure 6.*** *Mobility prediction scenario: slope traversal with zero degree steering angles. (a) A schematic view of the scenario and (b) tiltable test field with the rover test bed.*

stress angle, $c$ is the soil cohesion, $\phi$ is the soil internal friction, $j_x$ and $j_y$ are the soil shear deformations, and $k_x$ and $k_y$ are the soil deformation moduli.

From the aforementioned equations, it is obvious that the terrain uncertainties addressed in this article (cohesion $c$ and internal friction angle $\phi$) directly affect calculation of the normal and shear stresses and result in uncertainty in wheel–terrain contact force calculation.

Note that the wheeled vehicle model described in this section has been developed and validated in the range where the wheel slip ratio is from 0.0 to 1.0 and the wheel slip angle is from 0° to ±30°, as seen in [6].

## Simulation and Experimental Studies of Mobility Prediction Performance

In this section, the computational efficiency of (benchmark) SMC, LHSMC, and SRSM approaches are compared via simulation study. Then, an experimental study of the mobility prediction algorithm performance in two different terrains is described. The validity of the proposed technique is confirmed through the comparison between predicted and experimental motion paths of the rover.

### *Scenario Description*

As shown in Figure 6, the mobility prediction scenario is one of a four-wheeled rover traversing flat, sloped terrain with a side-slope angle of 10°, while maintaining 0° of steering angle at every wheel. The rover (see Figure 4) has dimensions of 0.44 m (length) × 0.30 m (width) × 0.30 m (height) and weighs approximately 13.4 kg in total. Each wheel has a diameter of 0.11 m and a width of 0.06 m. The angular velocity of each wheel is controlled to maintain 0.3 rad/s.

The coordinate system of the rover is described in Figure 7. The position and yaw orientation (heading) of the rover body are expressed based on a slope-coordinate system $\sum_s$. Kinematic and dynamic parameters of the rover are summarized in Tables 1 and 2, respectively.

The terrain surface of the slope is assumed to be evenly covered with two different types of soil: in Case A, the surface consists of the Lunar regolith simulant described in [25], whereas in Case B, it is covered with cohesionless, Toyoura sand provided by [26].

Uncertainties are represented in two critical terrain physical parameters: cohesion and internal friction angle. The mean and deviation of these parameters for the two soils of interest were determined by manual characterization and are summarized in Table 3. (Note that the mean and deviation can generally be estimated by engineering approximation or predicted to be similar to well-characterized soils.) Other parameters for the calculation of wheel–terrain interaction forces are summarized in Table 4.

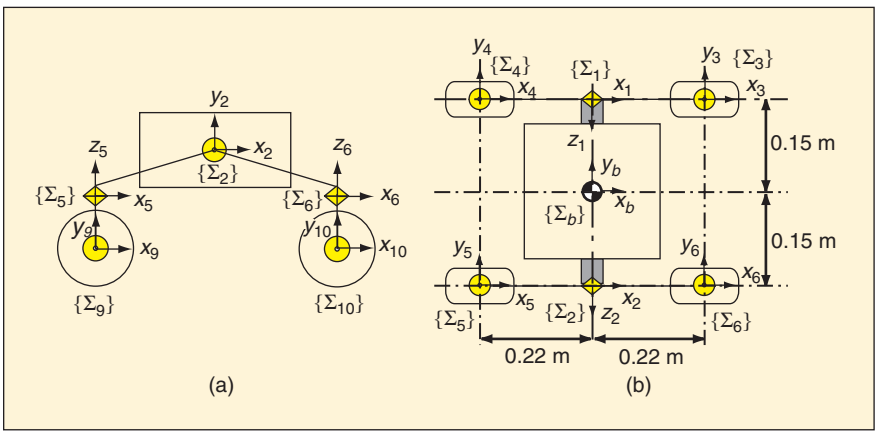


***Figure 7.*** *Coordinate system of the rover model. (a) Side and (b) top views.*

### *Algorithm Flow of Mobility Prediction Method*

Rover mobility is predicted following the flowchart in Figure 1. In this study, the probability distributions due to terrain uncertainty include the motion path during rover slope traversal, vehicle orientation, and wheel slippage.

The algorithm flow of the proposed mobility prediction method is summarized as follows:

1) choose a sample value for the standard normal random variables $\xi_c$ and $\xi_\phi$ and then calculate terrain parameters with uncertainty by (6)

2) conduct slope traversal simulations over the set of uncertain terrain parameters $\boldsymbol{G}_i$:
   a) determine $\tau$ such that the steering angle and wheel angular velocity are controlled to maintain their desired values
   b) derive the external forces $F_e$ acting at each wheel from the wheel–terrain contact model of (21)–(23)
   c) solve (18) to obtain the rover position, orientation, and velocity
   d) calculate the slip ratio and slip angle by (19) and (20).
3) return to Step 1 until sufficient data sets of the state space $\boldsymbol{X}$ for calculation of the unknown coefficients are obtained. Taking the number of model simulation trials $M$ to be approximately twice the number of unknown coefficients, $(N+1)$ has been shown to yield robust coefficient calculations [18], [20]
4) calculate the unknown coefficient matrices for the multidimensional Hermite polynomials using singular value decomposition and a regression-based approach
5) formulate a statistically equivalent reduced model as in (7) for the output uncertainty, and then predict the rover position, orientations, and wheel slippages
6) calculate confidence ellipses based on (14) and draw a motion path with ellipses for visualization purposes.

### *Simulation Results and Computational Efficiency*

Simulation results of the motion paths of the rover using SMC, LHSMC, and SRSM are shown in Figures 8 (Case A: Lunar regolith simulant) and 9 (Case B: Toyoura sand).

The solid black line shows the predicted motion path using SRSM. This consists of the mean value of the rover position ($x$ and $y$) calculated from the reduced model. In this case, the motion path obtained from SRSM is nearly identical to those obtained from SMC and LHSMC (solid gray and dashed black lines, respectively), making the results difficult to distinguish in the figures. In Figure 8, the difference between the rover's final positions, as computed by SRSM and SMC, was 0.001 m. In Figure 9, the difference between the rover's final positions, as computed by SRSM and SMC, was 0.002 m.

*A conventional technique for estimating probability density function of a system's output response from uncertain input distributions is the Monte Carlo method.*

The graphs also illustrate confidence ellipses with a probability $P = 95\%$ ($\approx 2\sigma$) in each predicted motion path. These ellipses of the three different approaches nearly coincide with one another. This indicates that the statistics such as variances and covariance obtained from SMC, LHSMC, and SRSM are also nearly identical. This result confirms that SRSM can provide a statistically equivalent representation of the complex system model considered in this analysis (i.e., the vehicle dynamic and wheel–terrain contact models).

Table 5 summarizes the computational time for mobility prediction between three approaches. The number of simulation runs of SMC was set as $n = 500$, while that of LHSMC was $n = 100$. The computational time of SRSM was approximately 71 times faster than that of SMC and 14 times faster than LHSMC. This is due to the fact that SRSM avoids multiple runs of the nonlinear model, which results in reduced simulation

**Table 1. Rover kinematic parameters.**

| Coordinate | *x* Axis (m) | *y* Axis (m) | *z* Axis (m) |
|---|---|---|---|
| $\sum_b \to \sum_1$ | −0.017 | 0.114 | −0.011 |
| $\sum_b \to \sum_2$ | −0.017 | −0.114 | −0.011 |
| $\sum_1 \to \sum_3, \sum_2 \to \sum_6$ | 0.222 | −0.050 | −0.035 |
| $\sum_1 \to \sum_4, \sum_2 \to \sum_5$ | −0.222 | −0.050 | −0.035 |
| $\sum_3 \to \sum_7, \sum_4 \to \sum_8$ | 0.000 | 0.045 | −0.071 |
| $\sum_5 \to \sum_9, \sum_6 \to \sum_{10}$ | 0.000 | −0.045 | −0.071 |

**Table 2. Rover dynamic parameters.**

| | Mass (kg) | Inertia (kg · m²) | | |
|---|---|---|---|---|
| | | $I_x$ | $I_y$ | $I_z$ |
| Main body $(\sum_b)$ | 7.17 | 0.064 | 0.104 | 0.095 |
| Rocker arm $(\sum_1, \sum_2)$ | 0.85 | 0.000 | 0.023 | 0.028 |
| Steering block $(\sum_3, \ldots, \sum_6)$ | 0.56 | 0.001 | 0.001 | 0.001 |
| Wheel $(\sum_7, \ldots, \sum_{10})$ | 0.58 | 0.001 | 0.001 | 0.001 |

**Table 3. Statistics of uncertain terrain parameters.**

| | Case A: Lunar Simulant | | Case B: Toyoura Sand | |
|---|---|---|---|---|
| Parameter | Mean | Std. Dev. | Mean | Std. Dev. |
| $c$ (kPa) | 8.0 | 1.0 | 0.08 | 0.01 |
| $\phi$(°) | 37.2 | 4.65 | 38.0 | 2.38 |

**Table 4. Terrain parameters and values.**

| | Value | | |
|---|---|---|---|
| Parameter | Case A: Lunar Simulant | Case B: Toyoura Sand | Unit |
| $k_c$ | 1.71 | 0.0 | – |
| $k_\phi$ | 4754.7 | 1203.5 | – |
| $\rho$ | 1700.0 | 1490.5 | kg/m³ |
| $n$ | 1.0 | 1.7 | – |
| $k_x$ | 0.104 | 0.077 | m |
| $k_y$ | 0.031 | 0.031 | m |

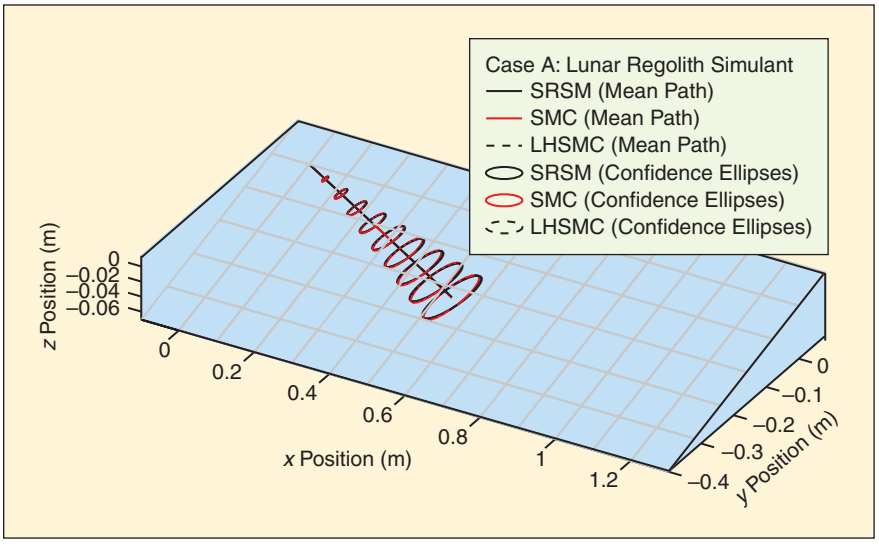


***Figure 8.*** *Mobility prediction with different approaches: SRSM, SMC, and LHSMC in Case A (Lunar regolith simulant).*

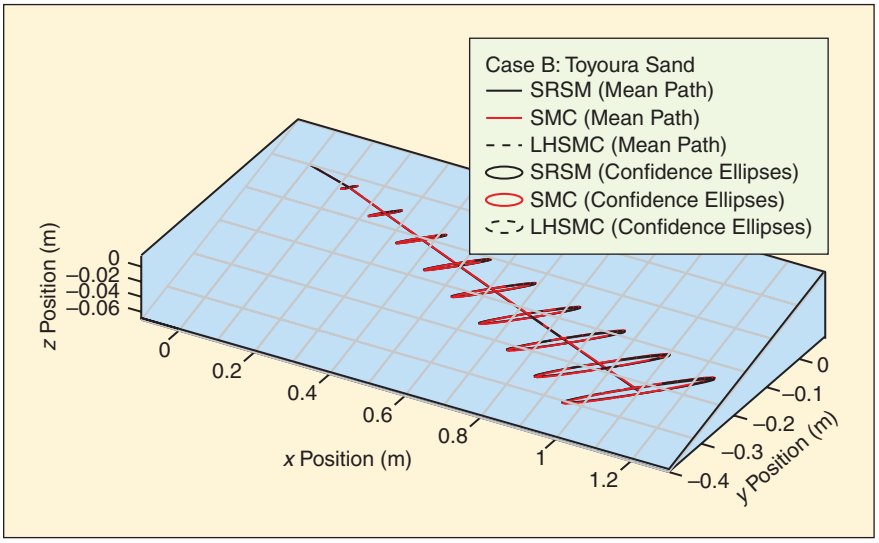


***Figure 9.*** *Mobility prediction with different approaches, SRSM, SMC, and LHSMC in Case B (Toyoura sand).*

time. Therefore, SRSM significantly improves the computational efficiency compared with conventional methods. These computations were performed on a 1.66-GHz laptop PC.

For onboard usage of the proposed method, the wheeled vehicle model can be simplified as long as it provides equivalent performance to the accurate model so that the computational time will be reduced further. For example, the linear approximation of wheel stress model reported in [7] can reduce the complexity of wheel–terrain contact model.

### *Experimental Results and Discussions*

Statistical mobility predictions of the motion paths of the rover on two different types of soil are shown in Figures 10 (Case A) and 11 (Case B) with experimental motion paths.

The predicted motion path of the rover obtained from SRSM is drawn as a gray line. Confidence ellipses were calculated with two different probabilities, $P = 68\%$ ($\approx 1\sigma$), drawn as black ellipses, and $P = 95\%$ ($\approx 2\sigma$), drawn as gray ellipses. These ellipses show the probable rover position considering uncertainty in terrain physical parameters. As expected, the $1\sigma$ confidence ellipses are smaller than the $2\sigma$ ellipses. The magnitude of the confidence level for mobility prediction can thus be tuned by the choice of probability.

The solid black line depicts the experimental motion path, which was obtained via laboratory experimentation. The path was measured using a motion-capture camera (Stereo Labeling Camera developed by CyVerse Corp.), with a positional accuracy of 0.01 m. Three experimental runs were performed for each soil. Here, a typical result among them is presented.

It can be seen that the rover reaches $(x, y) = (0.53, -0.18)$ in Case A and $(x, y) = (1.10, -0.26)$ in Case B, having a relatively large positional uncertainty because of the uncertainty in terrain parameters. Based on (15), the dimensions of the $2\sigma$ confidence ellipses can be calculated as $(a_x, a_y) = (0.06, 0.03)$ in Case A, and $(a_x, a_y) = (0.16, 0.01)$ in Case B. In both cases, the experimental motion path falls within the predicted

**Table 5. Computation time for mobility prediction analysis.**

| Method | Case A: Lunar Simulant | Case B: Toyoura Sand |
|---|---|---|
| SMC (500 runs) | 17526.1 s | 79994.1 s |
| LHSMC (100 runs) | 3507.2 s | 16232.5 s |
| SRSM (second order) | 245.8 s | 1125.9 s |

**Table 6. Mobility prediction results.**

| | Case A: Lunar Simulant | | Case B: Toyoura Sand | |
|---|---|---|---|---|
| Parameter | Mean | $2\sigma$ Dev. | Mean | $2\sigma$ Dev. |
| Roll (°) | 10.1 | 0.00 | 13.3 | 0.01 |
| Yaw (°) | −0.17 | 0.17 | 9.58 | 0.09 |
| Slip ratio | 0.43 | 0.03 | 0.29 | 0.08 |
| Slip angle (°) | −18.8 | 3.93 | −14.5 | 4.20 |

confidence ellipses, and in particular, the $1\sigma$ ellipses still contain the experimental results. This suggests that the proposed mobility prediction can be used to reasonably predict rover motion. Viewed from another perspective, the results suggest that the actual (i.e., experimental) terrain parameters lie within the assumed ranges.

Experimental results regarding the rover orientations (roll and yaw) and wheel slippage (at the front-left wheel of the rover) are summarized in Table 6. The predicted values include the uncertainty bounds on the $2\sigma$ deviations. The deviations of the vehicle orientations are negligible in both cases, indicating that terrain uncertainty does not have a significant influence on vehicle orientation in these cases.

The mean value of the wheel slip ratios are approximately 0.3–0.4, with small deviations in each case. However, the deviations of the slip angles are approximately 25% of their mean value. Since the deviation of the lateral wheel slip (measured by slip angle) is more significant than that of the longitudinal wheel slip (measured by slip ratio), deviation of the lateral vehicle position (depicted by the major axis of the confidence ellipses in Figures 10 and 11) is larger than that of the longitudinal vehicle position (depicted by the ellipses' minor axes). Thus, as expected, for the case of slope traversal, uncertainty in terrain parameters largely contributes to the deviation in the lateral direction of the rover rather than in the longitudinal direction.

SRSM models are generally constructed for specific scenarios. An SRSM model developed for a scenario (e.g., 10° downhill traverse) would not be used to model other scenarios (e.g., 20° traverse). However, it is possible to develop other SRSM models for other scenarios based on the proposed method, because generation of an SRSM model is relatively computationally inexpensive. In addition, an SRSM model is generally constructed for a particular scenario to include estimates of variability in that scenario. In the application studied here, this includes variability in soil parameters.

## Conclusions

In this article, a statistical mobility prediction for planetary surface exploration rovers has been described. This method explicitly considers uncertainty of the terrain physical parameters via SRSM and employs models of both vehicle dynamics and wheel–terrain interaction mechanics.

The simulation results of mobility prediction using three different techniques, SMC, LHSMC, and SRSM, confirms that SRSM significantly improves the computational efficiency compared with those conventional methods.

***SRSM is used as a functional approximation technique to obtain an equivalent system model with reduced complexity.***

The usefulness and validity of the proposed method has been confirmed through experimental studies of the slope-traversal scenario in two different terrains. The results show that the predicted motion path with confidence ellipses can be used as a probabilistic reachability metric of the rover position. Also, for the slope-traversal case, terrain parameter uncertainty has a larger influence on the lateral motion of the rover than on longitudinal motion.

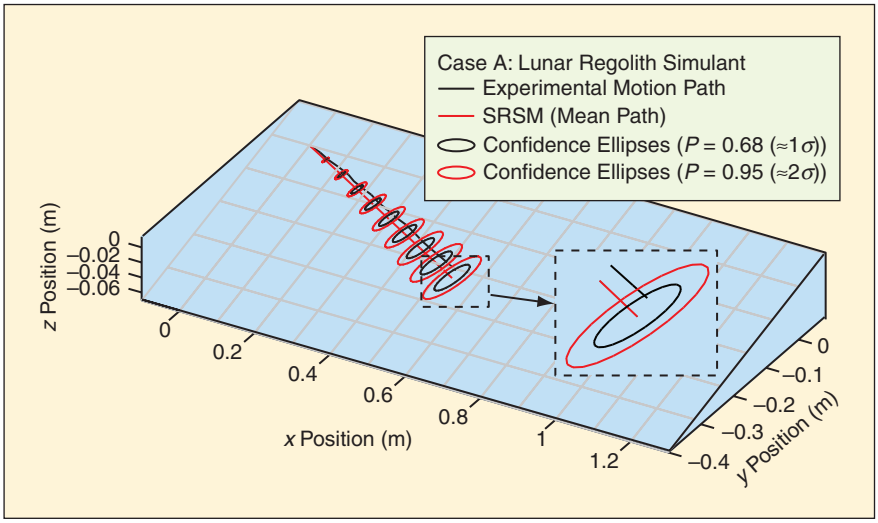


***Figure 10.*** *Mobility prediction of motion path with confidence ellipses, $P = 68\%$ ($\approx 1\sigma$) and $P = 95\%$ ($\approx 2\sigma$) in Case A (Lunar regolith simulant).*

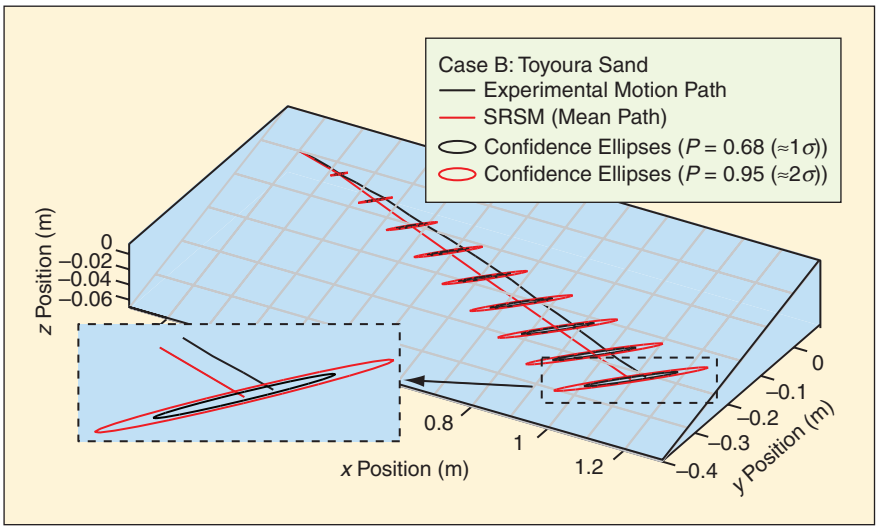


***Figure 11.*** *Mobility prediction of motion path with confidence ellipses, $P = 68\%$ ($\approx 1\sigma$) and $P = 95\%$ ($\approx 2\sigma$) in Case B (Toyoura sand).*

***Monte Carlo methods are well-known techniques for estimating a probability distribution of a system's output response from uncertain input parameters.***

Future directions of this study will apply the proposed technique to the path-planning problem. Here, confidence ellipses will be used to define collision-free areas, which will provide useful criteria for generating safe trajectories.


## Keywords

Field robots, space robotics, wheeled robots.


## References


[1] (2009, Oct.). Mars exploration Rover mission [Online]. Available: http://marsrovers.jpl.nasa.gov/home/index.html

[2] M. Jurkat, C. Nuttall, and P. Haley, "The AMC '74 mobility model," US Army Tank Automotive Command, Warren, MI, Tech. Rep. 11921, 1975.

[3] R. B. Ahlvin and P. W. Haley, "NATO reference mobility model edition II, NRMM user's guide," U.S. Army WES, Vicksburg, MS, Tech. Rep. GL-92-19, 1992.

[4] A. Jain, J. Guineau, C. Lim, W. Lincoln, M. Pomerantz, G. Sohl, and R. Steele, "ROAMS: Planetary surface rover simulation environment," in *Proc. 7th Int. Symp. Artificial Intelligence, Robotics and Automation in Space, i-SAIRAS*, Nara, Japan, May 19–23, 2003, No. AM31.

[5] A. Gibbesch and B. Schäfer, "Multibody system modelling and simulation of planetary rover mobility on soft terrain," in *Proc. 8th Int. Symp. Artificial Intelligence, Robotics and Automation in Space, i-SAIRAS*, Munich, Germany, Sept. 5–8, 2005, No. 03a-1.

[6] G. Ishigami, A. Miwa, K. Nagatani, and K. Yoshida, "Terramechanics-based model for steering maneuver of planetary exploration rovers on loose soil," *J. Field Robot.*, vol. 24, no. 3, pp. 233–250, 2007.

[7] K. Iagnemma, S. Kang, H. Shibly, and S. Dubowsky, "Online terrain parameter estimation for wheeled mobile robots with application to planetary rovers," *IEEE Trans. Robot.*, vol. 20, no. 5, pp. 921–927, 2004.

[8] J. R. Matijevic, J. Crisp, D. B. Bickler, R. S. Banes, B. K. Cooper, H. J. Eisen, J. Gensler, A. Haldemann, F. Hartman, K. A. Jewett, L. H. Matthies, S. L. Laubach, A. H. Mishkin, J. C. Morrison, T. T. Nguyen, A. R. Sirota, H. W. Stone, S. Stride, L. F. Sword, J. A. Tarsala, A. D. Thompson, M. T. Wallace, R. Welch, E. Wellman, B. H. Wilcox, D. Foerguson, P. Jenkins, J. Kolecki, G. A. Landis, and D. Wilt, "Characterization of Martian surface deposits by the Mars pathfinder rover, Sojourner," *Science*, vol. 278, no. 5, pp. 1765–1768, 1997.

[9] S. Hutangkabodee, Y. Zweiri, L. Seneviratne, and K. Althoefer, "Soil parameter identification for wheel—terrain interaction dynamics and traversability prediction," *Int. J. Automat. Comput.*, vol. 3, no. 3, pp. 244–251, 2006.

[10] D. Helmick, A. Angelova, L. Matthies, C. Brooks, I. Halatci, S. Dubowsky, and K. Iagnemma, "Experimental results from a terrain adaptive navigation system for planetary rovers," in *Proc. 9th Int. Symp. Artificial Intelligence, Robotics and Automation in Space, i-SAIRAS*, Hollywood, CA, no. 110, Feb. 26–29, 2008.

[11] R. Rubinstein, *Simulation and the Monte Carlo Method*. New York: Wiley, 1981.

[12] M. Kalos and P. Whitlock, *Monte Carlo Methods*, vol. 1, *Basics*. New York: Wiley-Interscience, 1986.

[13] M. D. McKay, "Latin hypercube sampling as a tool in uncertainty analysis of computer models," in *Proc. 24th Conf. Winter Simulation*, 1992, pp. 557–564.

[14] J. C. Helton and F. J. Davis, "Latin hypercube sampling and the propagation of uncertainty in analyses of complex systems," *Reliab. Eng. Syst. Saf.*, vol. 81, no. 1, pp. 23–69, 2003.

[15] S. Thrun, D. Fox, W. Burgard, and F. Dellaert, "Robust Monte Carlo localization for mobile robots," *Artif. Intell. J.*, vol. 128, no. 1–2, pp. 99–141, 2001.

[16] D. Fox, "Adapting the sample size in particle filters through KLD-sampling," *Int. J. Robot. Res.*, vol. 22, no. 12, pp. 985–1004, 2003.

[17] S. Isukapalli, S. Balakrishnan, and P. Georgopoulos, "Computationally efficient uncertainty propagation and reduction using the stochastic response surface method," in *Proc. IEEE Conf. Decision and Control*, Atlantis, Bahamas, Dec. 14–17, 2004, pp. 2237–2243.

[18] S. Isukapalli, "Uncertainty analysis of transport-transformation models," Ph.D. thesis, Rutgers State Univ. of New Jersey, New Brunswick, NJ, 1999.

[19] G. Kewlani and K. Iagnemma, "Mobility prediction for unmanned ground vehicles in uncertain environments," in *Proc. SPIE Conf. Unmanned Systems Technology*, 2008, vol. 6962, pp. 69621G-1–69621G-12.

[20] S. Huang, S. Mahadevan, and R. Rebba, "Collocation-based stochastic finite element analysis for random field problems," *Probab. Eng. Mech.*, vol. 22, no. 2, pp. 194–205, 2007.

[21] L. Li and C. Sandu, "On the impact of cargo weight, vehicle parameters, and terrain characteristics on the prediction of traction for off-road vehicles," *J. Terramech.*, vol. 44, no. 3, pp. 221–238, 2007.

[22] L. R. Paradowski, "Uncertainty ellipses and their application to interval estimation of emitter position," *IEEE Trans. Aerosp. Electron. Syst.*, vol. 33, no. 1, pp. 126–133, 1997.

[23] M. G. Bekker, *Introduction to Terrain-Vehicle Systems*. Ann Arbor, MI: Univ. of Michigan Press, 1969.

[24] J. Y. Wong, *Theory of Ground Vehicles*, 3rd ed. New York: Wiley, 2001.

[25] H. Nakashima, Y. Shioji, K. Tateyama, S. Aoki, H. Kanamori, and T. Yokoyama, "Specific cutting resistance of Lunar Regolith. Simulant under low gravity conditions," *J. Space Eng.*, vol. 1, no. 1, pp. 58–68, 2008.

[26] (2009, Oct.). Toyoura Keiseiki Kogyo Co., Ltd. [Online]. Available: http://www.toyourakeiseki.com/product-e.htm



**Genya Ishigami** received his M.Eng. and Ph.D. degrees from Tohoku University, Japan, in 2005 and 2008, respectively. He is currently a postdoctoral associate in the Mechanical Engineering Department at the Massachusetts Institute of Technology (MIT). His research interests are in the areas of mobility analysis, including vehicle-terrain interaction mechanics, design, planning, and control, and for the application to planetary exploration rovers, rescue robots, and field robots.

**Gaurav Kewlani** received his B.Tech. degree in mechanical engineering from the Indian Institute of Technology, Delhi, in 2007 and his S.M. degree in mechanical engineering from MIT in 2009. His research interests include efficient mobility prediction and path planning for mobile robotic systems, design and dynamics of mechanical systems, as well as product design and development.

**Karl Iagnemma** received his B.S. degree from the University of Michigan and M.S. and Ph.D. degrees from MIT. He is a director of the Robotic Mobility Group at MIT. He is the author of the book *Mobile Robots in Rough Terrain: Estimation, Planning and Control with Application to Planetary Rovers* (Springer, 2004). He is currently an associate editor of *IEEE Transactions on Robotics* and *Journal of Field Robotics*.

***Address for Correspondence:*** Genya Ishigami, Massachusetts Institute of Technology, 77 Massachusetts Avenue, Room 35-135A, 02139 Cambridge, MA, USA. E-mail: ishigami@mit.edu.